This is the submitted version of the article:

Zamani M., Tütüncüoglu G., Martí-Sánchez S., Francaviglia L., Güniat L., Ghisalberti L., Potts H., Friedl M., Markov E., Kim W., Leran J.-B., Dubrovskii V.G., Arbiol J., Fontcuberta I Morral A.. Optimizing the yield of A-polar GaAs nanowires to achieve defect-free zinc blende structure and enhanced optical functionality. Nanoscale, (2018). 10. : 17080 - . 10.1039/c8nr05787g.

Available at: https://dx.doi.org/10.1039/c8nr05787g

Nanoscale

Maximizing the yield of A-polar GaAs nanowires to achieve a single-phase structure and enhanced functionality

Journal:	*Nanoscale*
Manuscript ID	Draft
Article Type:	Paper
Date Submitted by the Author:	n/a
Complete List of Authors:	Zamani, Mahdi; Ecole Polytechnique Federale de Lausanne, Institute of Materials Tütüncüoglu, Gözde; Ecole Polytechnique Federale de Lausanne, Institute of Materials Martí-Sánchez, Sara; Catalan Institute of Nanoscience and Nanotechnology (ICN2), CSIC and BIST, Campus UAB, Bellaterra Francaviglia, Luca; Ecole Polytechnique Federale de Lausanne, Laboratoire des Matérieux Semiconducteurs Markov, Edoardo; Ecole Polytechnique Federale de Lausanne, Institute of Materials Kim, Wonjong; Ecole Polytechnique Federale de Lausanne, Institute of Materials Güniat, Lucas; Ecole Polytechnique Federale de Lausanne, Institute of Materials Ghisalberti, Lea; Ecole Polytechnique Federale de Lausanne, Institute of Materials Potts, Heidi; Laboratory of Semiconductor Materials, IMX Friedl, Martin; Ecole Polytechnique Federale de Lausanne, Institute of Materials Leran, Jean-Baptiste; Ecole Polytechnique Federale de Lausanne, Institute of Materials Dubrovskii, V. G. ; St. Petersburg Academic University, Laboratory of Physics of Nanostructures Arbiol, Jordi; Institut Català de Nanociència i Nanotecnologia (ICN2), CSIC and The Barcelona Institute of Science and Technology (BIST), Advanced Electron Nanoscopy (GAeN); ICREA, Fontcuberta i Morral, Anna; Ecole Polytechnique Federale de Lausanne, Institute of Materials

SCHOLARONE™
Manuscripts

Please do not adjust margins

Nanoscale

ARTICLE

Optimizing the yield of A-polar GaAs nanowires to achieve defect-free zinc blende structure and enhanced optical functionality

Received 00th January 20xx,
Accepted 00th January 20xx

DOI: 10.1039/x0xx00000x

www.rsc.org/

Mahdi Zamani, [a†] Gözde Tütüncüoglu, [a†] Sara Martí-Sánchez, [b] Luca Francaviglia, [a] Lucas Güniat, [a] Lea Ghisalberti, [a] Heidi Potts, [a] Martin Friedl, [a] Edoardo Markov, [a] Wonjong Kim, [a] Jean-Baptiste Leran, [a] Vladimir G. Dubrovskii, [d] Jordi Arbiol, [b,c] Anna Fontcuberta i Morral [a]*
[†]equal contribution, *corresponding author

Compound semiconductors exhibit an intrinsic polarity, as a consequence of the ionicity of their bonds. Nanowires grow mostly along the (111) direction for energetic reasons. Arsenide and phosphide nanowires grow along (111)B, implying a group V termination of the (111) bilayers. Polarity engineering provides an additional pathway to modulate the structural and optical properties of semiconductor nanowires. In this work, we demonstrate for the first time the growth of Ga-assisted GaAs nanowires with (111)A-polarity, with a yield of up to ~50%. This goal is achieved by employing highly Ga-rich conditions which enable proper engineering of the energies of A and B-polar surfaces. We also show that A-polarity growth suppresses the stacking disorder along the growth axis. This results in improved optical properties, including the formation of AlGaAs quantum dots with two orders or magnitude higher brightness. Overall, this work provides new grounds for the engineering of nanowire growth directions, crystal quality and optical functionality.

Introduction

Semiconductor nanowires (NWs) have gained increasing interest due to unique properties arising from their one-dimensional morphology and functionalities enabled by their characteristic growth mechanism. [1-14] The most common technique for NW growth is the vapor-liquid-solid (VLS) method, in which a liquid droplet collects precursors from the vapor phase to then precipitate them at the interface with the solid[1]. Most commonly, gold is used as the VLS growth catalyst,[2–5] however, it may contaminate NWs.[6] Ga-assisted growth, otherwise known as self-catalyzed growth, overcomes this challenge for GaAs. [7–14]

An intrinsic property of compound semiconductors is their polarity. This term refers to the electric dipole of the bonds, originating from the different electron affinity of the composing elements. The sign and magnitude of this finite electrical field depends on the crystal direction. Compound semiconductor NWs tend to grow in the <111> directions. (111) surfaces are composed by bi-layers of III-V dumbbells with an intrinsic electric field normal to the surface. When the surface is terminated by a group III or V element, it is named (111)A and (111)B, respectively. Recent developments in electron microscopy allow for a relatively straightforward determination of the polarity of NW growth direction.[15–17] NWs tend to grow with a prevalent polarity, depending on the material. For example, Ga(N,P,As), In(N,P,As,Sb) and Zn(S,Se,Te) tend to grow along the <111>B direction, while ZnO shows mostly <111>A-polarity.[15–21]

Recently, it has been shown that the structural properties of compound semiconductor NWs can vary significantly when their growth direction and polarity are modified.[22] In bulk, GaAs exhibits zinc blende (ZB) structure, while the presence of polytypism and wurtzite phase (WZ) in (111)B-polar GaAs NWs is well documented.[23–25] Few groups have assessed the engineering of crystal growth polarity by modifying the contact angle of the VLS droplet. Yuan et al demonstrated for the first time that modifying the droplet wetting and surface energy allowed for the switching of the polarity of Au-catalyzed GaAs NWs from the usual B to A.[26] According to their study, A-polar NWs are obtained with higher contact angles, which they explained by the higher surface energy of A-polar surfaces. The presence of rotational twins[27] and polytypism typically observed in B-polar NWs as completely suppressed in A-polar NWs. This

[a] Laboratoire des Matériaux Semiconducteurs, École Polytechnique Fédérale de Lausanne, EPFL, 1015 Lausanne, Switzerland Address here.
[b] Catalan Institute of Nanoscience and Nanotechnology (ICN2), CSIC and BIST, Campus UAB, Bellaterra, 08193 Barcelona, Catalonia, Spain
[c] ICREA, Pg. Lluís Companys 23, 08010 Barcelona, Catalonia, Spain
[d] ITMO University, Kronverkskiy prospekt 49, 197101 St. Petersburg, Russia
*email: anna.fontcuberta-morral@epfl.ch

Please do not adjust margins

was an important finding as it opened the path toward growth of defect-free GaAs NWs. Another recent study showed similar results on Sn-seeded GaSb NWs.[28] In this case, the A- polar NWs were defect-free, in contrast to the B-polar NWs which had spaced stacking defects appearing in the <111>A direction. The presence of these defects resulted in zigzag-shaped sidewalls in B-polar NWs.

In this work, we demonstrate for the first time that GaAs NWs can be grown reliably grown in the <111>A direction by the Ga-assisted VLS method. This shows that catalyst for growth of A-polar GaAs NWs does not need to be restricted to gold. This observation is significant, because gold-assisted growth is not compatible with the existing semiconductor industry. We provide a parametric study on the occurrence of the two polarities as a function of Ga and As_4 fluxes and substrate temperature. The detailed study of the crystal structure of NWs having different polarities is performed by aberration-corrected high-angle annular dark field scanning transmission electron microscopy (AC-HAADF-STEM). The relation between the nanowire polarity and the optical properties have been studied by low temperature cathodoluminescense (CL).

Experimental details

First, the GaAs (100) substrates were etched in HF to remove the native oxide. The silicon oxide layers were obtained by spin coating a solution of Hydrogen Silsesquioxane (HSQ) and Methyl Isobutyl Ketone (MIBK). The spin-coated layers were annealed at 300 °C for 10 minutes. The oxide thicknesses used for all the samples were around 3.3 nm. Two additional annealing steps at 150°C and 300°C for two hours each were performed inside the MBE chamber. The initial chamber pressure for all the growths was less than 5×10^{-10} Torr. For the sample discussed in Figure 6, the growth conditions for the NW core were: the V/III ratio of 1.9, 2D growth rate of 0.24 Å/s, at a substrate temperature of 640 °C. The growth conditions for the shell were: As flux of 9.3×10^{-6} mbar, 2D growth rate of 0.7 Å/s, substrate temperature of 450 °C.

The TEM samples were prepared by scraping a TEM grid on an as-grown sample.[29] Atomic resolution HAADF-STEM was performed in a probe corrected FEI Titan 60-300 keV microscope operated at 300 keV. TEM images given in Figure 5 were obtained with an FEI Talos machine operating at 200 keV.

The CL measurements were performed using an Attolight Rosa 4634 SEM-CL microscope at the Interdisciplinary Center for Electron Microscopy (CIME), EPFL. The measurements reported in Figure 5(h) and 6(a) were performed using a beam accelerated to 5 keV, while for the measurements in Figure 6(i) and 5(j) this value was 8 keV. For all the measurements, the acquisition time of each spectra was 0.1 s and the beam current was on the order of 1 nA.

Results and Discussion

Polarity in compound semiconductor NWs can be determined in an unambiguous manner by identifying the atomic columns in the material, typically using AC-HAADF-STEM techniques.[22] These techniques are precise at the atomic level but incompatible with a fast statistical assessment on a large ensemble of NWs. Alternatively, the NW growth polarity can be determined by their orientation with respect to the epi-substrate, which in our case is GaAs(100). Figure 1 represents the atomic arrangement of NWs oriented along the <111>A and <111> B with respect to such substrate. In the insets, we provide the details of atomic order when looking along the [-110] and [110] zone axes, respectively. We have assessed the polarity of NWs in ensembles by correlating their orientation with the crystalline axes of the substrate using top view SEM micrographs.

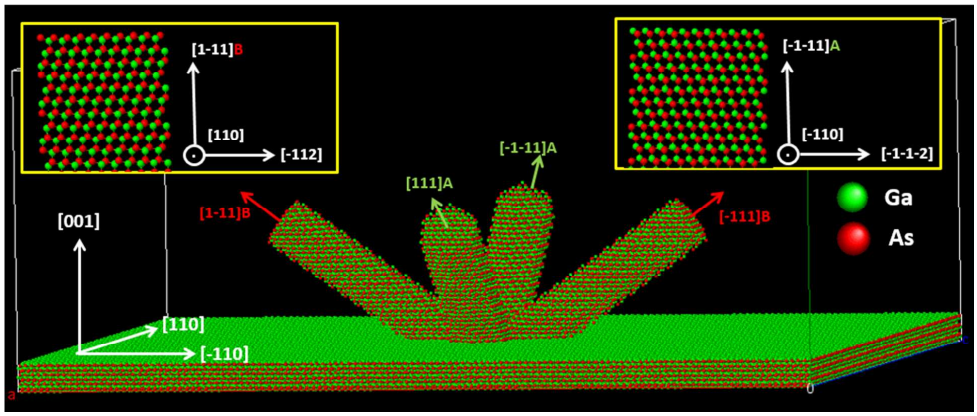

Figure 1. Three-dimensional atomic model of GaAs NWs oriented along the <111>B and <111>A directions on a GaAs(100) substrate. The insets zoom in the atomic ordering in the [110] and [-110] zone axis, respectively, for B and A-polar NWs.

Figure 2(a) shows a representative top-view scanning electron microscope (SEM) image of one of the grown samples. Here, the NW projections appear oriented along the two perpendicular directions, which correspond to the <111>A and <111>B

This journal is © The Royal Society of Chemistry 20xx

Please do not adjust margins

directions. A closer look at this image reveals the presence of NWs crawling on the surface. Similar structures were previously observed in the VLS growth of NWs.[30] A low V/III ratio yields the formation of big droplets, which can easily be unpinned from the top of the structures in the early stages of growth and fall down onto the substrate. The subsequent growth originating from such droplets will result in the formation of crawling structures.[31] Increased oxide thickness or hole density might prevent the appearance of crawling objects.[32–35] Figures 2(b) and (c) show the cross-sectional SEM images of another sample in the two perpendicular cleaving directions. One can distinguish the two NW populations also in this configuration. As expected, the angle of the NWs with respect to the substrate normal is 54.5°.

We have studied the ratio between number of the B and A-polar NWs as a function of the growth parameters. For this, we have kept the substrate temperature at 640 °C and modified the V/III ratio and the Ga flux. Statistics of the population of A-polar NWs obtained from examining the top-view SEM images is shown in Figure 2(d). We observe an increase in the population of A-polar NWs when reducing the V/III ratio. This effect will be discussed shortly. Unexpectedly, the Ga flux itself also affects the A/B ratio, with an optimum value being around 0.21-0.24 Å /s. It was not possible to distinguish the two polarities in the range of grey data points due to the shorter lengths of the nanowires.

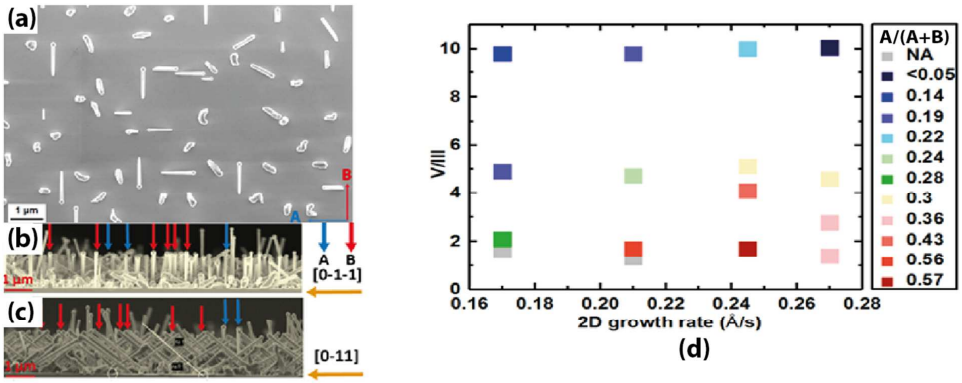

Figure 2. (a) Top view SEM image of a sample grown with a Ga rate of 0.21 Å /s and a V/III ratio of 1.7. The colored arrows indicate the projections corresponding to <111>A and <111>B directions. (b) and (c) Cross-sectional SEM images of a sample grown with a Ga rate of 0.60 Å/s and a V/III ratio of 2.9, cleaved along the two <100> directions The colored arrows indicate the NW polarity (A or B) according to their orientation with respect to the (100) GaAs substrate. (d) Fraction of A-polar NWs as a function of V/III ratio and the 2D equivalent Ga growth rate. There is a clear increase in A-polar NW fraction when the V/III ratio is reduced. In addition, the Ga flux itself also affects the fraction of A-polar NWs, with a clear maximum in the range of 0.21-0.24 Å/s.

From Fig. 2 (b), we see that the fraction of A-polar NWs can be tuned to 0.57 for V/III ratios of around 2 and Ga rates of 0.21-0.24 Å/s. We note that the growth conditions leading to the highest yield of A-polar NWs on GaAs(100) substrates do not work on (111)A substrates. Instead, NWs crawling on the substrate surface was mostly observed on (111)A under similar conditions. We attribute this result to the different wetting properties of the Ga droplet on (100), (111)B and (111)A surfaces.

These results indicate a competition between the nucleation of A and B-polar GaAs NWs on GaAs(100) substrates, where the A-polarity is preferred at low V/III ratios. A quantitative description of the nucleation probabilities for NWs with different parameters under different Ga and As_4 fluxes requires a separate study and will be presented elsewhere. Here we just mention that the liquid droplet catalyzing the VLS growth of any NWs should wet the growth front but not the NW sidewalls.[26,28,36] In general, (111)A facets are rarely seen as the growth front in a nanowire. One reason could be that their surface energy would be higher than for (111)B and hence their formation would be energetically and geometrically suppressed in favor of the (111)B facets.[31,37,38] The (111) surface energy as well as the nucleation probability of GaAs is also affected by kinetic or thermodynamic factors such as chemical potential in the liquid phase.[2,42] It is very possible that a reduction in the As concentration under lower As fluxes causes the effective energies of A and B surfaces to decrease and increase, respectively. This reduction results in increasing the wetting chance of an A-polar surface with respect to a B-polar surface. For this reason, lowering the V/III ratio could increase the probability of wetting A-polar surfaces and hence growing A-polar NWs. We note that the previous attempts to grow A-polar GaAs and GaSb NWs (gold and tin-catalyzed, respectively)[26,28] used a similar strategy for increasing the wettability of A-polar surfaces, although without changing the V/III ratio to achieve this goal. The coexistence of NWs of different polarities can be explained by the fact that the modification in the energy of A-polar surfaces might not be enough to make the wetting of the B-polar surfaces completely

Please do not adjust margins

Please do not adjust margins

unfavorable.[26,28] The highest yield of A-polar NWs corresponds to extremely low As_4 fluxes. Further decrease of the As_4 input cannot be achieved in a reproducible manner because the lowest flux is already close to the background pressure under our growth conditions. Hence, it is not possible to further reduce the V/III ratio to obtain a higher yield of A-polar NWs.

Changing the V/III ratio strongly affects the contact angle of Ga droplets seated on top of developed NWs. Recently, contact angle engineering has been used to tune the growth direction and polarity of NWs.[26,39] The contact angles and the growth interfaces of our A and B-polar GaAs NWs will be discussed shortly.

We now turn to the analysis of the polarity by AC-HAADF-STEM. Unless otherwise stated, the NWs considered here are covered with an $AlAs/Al_{0.33}Ga_{0.67}As/GaAs$ shell heterostructure with nominal thicknesses of 10 nm /100 nm /10 nm respectively. $Al_{0.33}Ga_{0.67}As$ shell is previously shown to contain self-assembled (Al)GaAs quantum dots (QDs) [40] whose optical properties are affected by the polarity. The $AlAs$ and the final $GaAs$ layers are used for enhancement of the QD formation[50] and protection of $Al_{0.33}Ga_{0.67}As$ against oxidation, respectively. Figure 3(a) shows the low magnification STEM image of a NW. Figure 3(b) shows atomically resolved AC-HAADF-STEM image of the middle part of the NW, demonstrating its defect-free crystal structure. Figure 3(c) shows the profile intensity scan in the direction of the arrow shown in the inset of Figure 3(b). This figure indicates that dumbbells are terminated by Ga/Al, confirming that this NW is A-polar. The crystal quality in the bulk of the NW is similar to the section shown in Figure 3(b), except for the parts at the base which correspond to the initial stages of growth. Figure 3(d) shows the neighboring sections of A, B and mixed polarities. The zoomed-in image of such sections is presented in Figure 3(e). The atomically resolved detail of the mixed section is shown in Figure 3(f), indicating 9R Ramsdell polytypism.[41] The step in the (111) ortho-twin boundary that forms a coherent, six monolayers high $\Sigma = 3$ (1-12) para-twin facet is also observed in Figure 3(g). The three monolayer step shows that the polarity across the {111} plane is preserved on each side of the step and that the atomic arrangements on the opposite sides of the (1-12) facet are related by a mirror symmetry. The As atoms form an As−As bond, while the As and Ga atoms on the boundary plane become 5-fold and 3-fold coordinated, as shown previously by Sanchez et al. In this work, a very similar type of defect was observed in (111)B GaAs(P) NWs. It was deemed to be detrimental to the functional properties of the structure, as it can act as a non-radiative recombination center.[42] The NW base also presents twins perpendicular to the growth axis, as in Figure 3(g). These twins do not result in switching the polarity of the NW, which otherwise would imply the formation of an electrostatic potential barrier that scatters the carriers and reduces their mobility.[15]

The twins present at the base of the NW are in stark contrast with the defects shown in Figure 3(h), in which we show the occurrence of lateral twins.[43] These defects flip the polarity from A and B along the NW growth direction, but not across the twin boundary. This type of lateral twin is commonly observed in {111} grown non-polar NWs (e.g., in Ga-catalyzed Si NWs).[43] In our GaAs NWs, twins mostly occur along a B-polar direction, meaning that in a B-polar NW, the twins observed will be perpendicular to the growth direction. In A-polar NWs, these twin boundaries will mainly occur along one of the three possible B-polar lateral facets, inclined 19° with respect to the <111>A direction. Furthermore, as the lateral twins are inclined with respect to the NW growth direction, although the polarity is always kept across the twin boundary, their presence implies a switch of polarity along the NW growth axis. Rarely, it is also observed that this sequence of defects can occur multiple times. As a general rule, we never observe twin defects perpendicular to the growth axis in A-polar NWs except in rare cases discussed below, demonstrating that the twinning tends to always occur along a B-polar direction. Based on the information given in Figure 3, we conclude that A-polar NWs are almost defect-free along most of their length. In these regions, defects only occur along the lateral sides in rare cases, where the twinned region expands along the B direction versus the NW edge and quickly extinguishes. Formation of rotational or transversal twins perpendicular to the axis of A-polar NWs is even more rare, and is just observed at the root of the NW, where A and B-polar growth fronts are competing. The only observations of WZ phase in A-polar NWs are limited to the cases in which twins were formed, as each twin in ZB crystal is equivalent to a half monolayer of WZ phase.[44] A continuous WZ section is never observed in A-polar NWs.

This journal is © The Royal Society of Chemistry 20xx

Please do not adjust margins

Please do not adjust margins

Nanoscale

ARTICLE

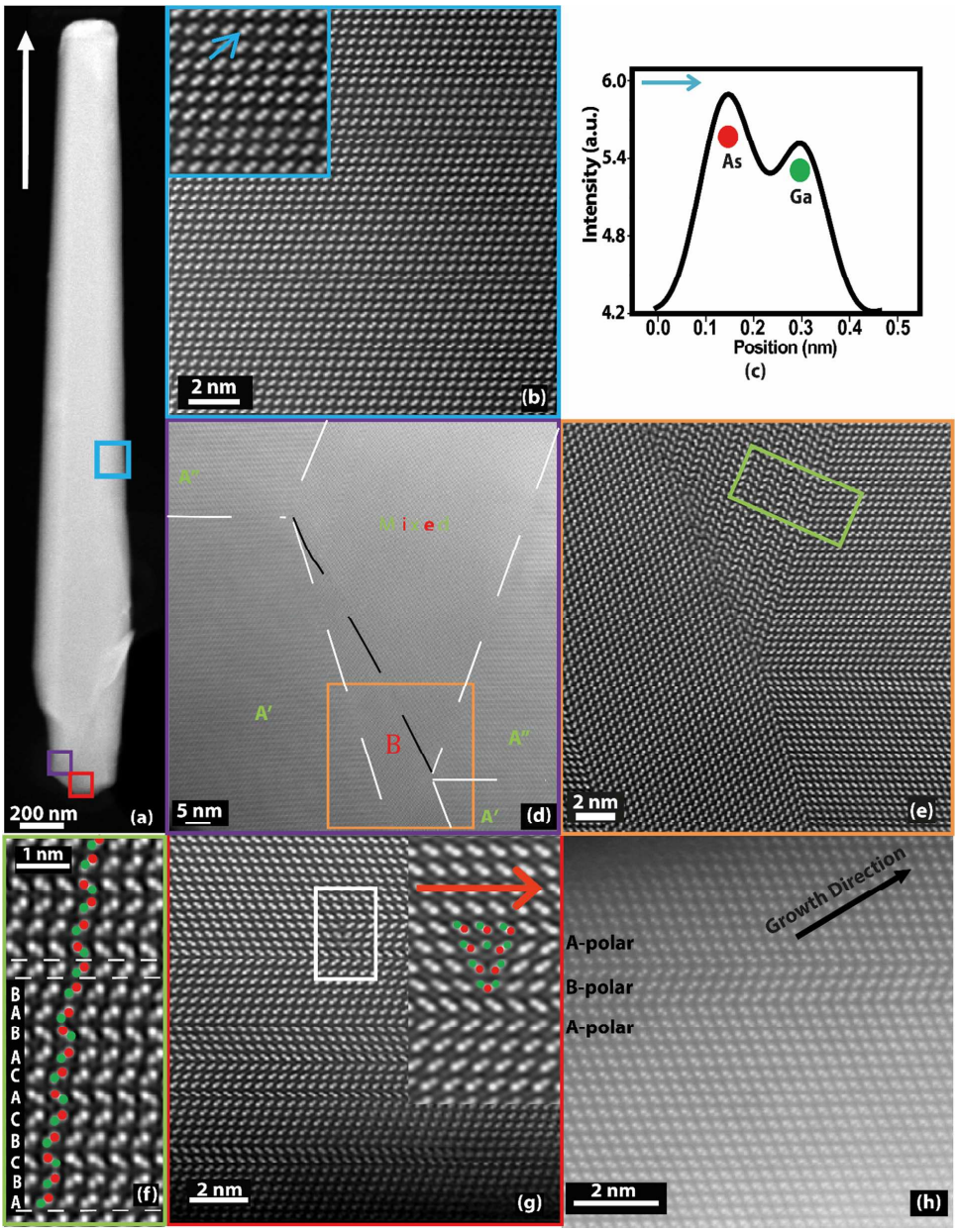

Please do not adjust margins

Please do not adjust margins

Figure 3: Structural characterization of A-polar NWs. (a) Low magnification STEM image of an A-polar NW. The white arrow indicates the growth direction, which is the same for images in (a) to (g). (b) The crystal structure of the generic blue frame shown in Figure 3(a). (c) Profile intensity scan in the direction of the arrow in Figure 3(b), confirming the A-polar nature of the NW. (d) Competing regions of A and B-polar growths at the root of the NW. (e) Magnified image of the orange box in Figure 3(d). (f) Magnified image of the green box shown in Figure 3(e), showing 9R Ramsdell polytypism. (g) The presence of twins perpendicular to A-polar growth direction, and the detail of a step in a (111) ortho-twin boundary; this defect is responsible for the in-plane polarity reversal. (h) The appearance of inclined twins in an A-polar NW. The black arrow shows the growth direction. Note that this image is from a different NW than the one shown in Figures 3(a) to 3(g).

A closer look at the internal atomic structure of a B-polar NW is shown in Figure 4. Figure 4(a) shows the low magnification image of a NW. Figures 4(b) and (c) give the atomically resolved crystal structure. The intensity profile scan along the arrow shown in Figure 4(c) confirms that the dumbbells are terminated by As, showing that the NW is B-polar. Indeed, the presence of rotational/transversal twins, typical of B-polar GaAs NWs, is observed in Figures 4(b) and 4(c). Unlike A-polar NWs, long WZ regions are easily observed in B-polar NWs, as depicted in Figure 4(e). Switching of polarity to A is locally observed in just one occasion, shown in Figure 4(f), in which the presence of a notch-like defect induces the formation of a lateral twin that propagates to the top of the NW. This creates a section of A-polar lateral growth on the NW side. Note that the polarity is always preserved across the twin boundary, but changes along the growth front on both sides of the twin boundary. This latter effect of a lateral twin defect propagating to the top of the NW with A-polarity, parallel to the main B-polarity of the NW, is similar to the lateral twins that induce the formation of nanosail-like InSb structures on top of InAs NW stems.[18] Figure 4(g) depicts the configuration of the neighbouring A and B-polar sections under the Ga droplet. The A-polar section originates at the notch-like defect found below. In short, unlike in the A-polar case, B-polar NWs show a high density of transversal twins and alternating sections of ZB/WZ phases. In addition, B-polar NWs very rarely show the formation of notch-like defects that alter the polarity to A by nucleating a lateral twin.

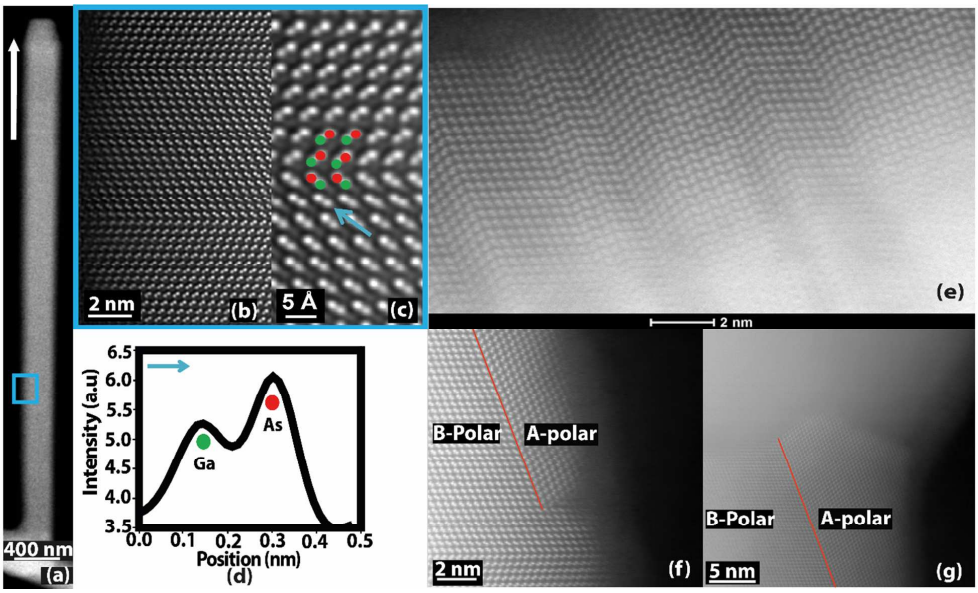

Figure 4: HAADF-STEM structural characterization of NWs with B-polarity. (a) Low magnification HAADF STEM image of a NW. (b) and (c) Atomically resolved details of the blue frame shown in Figure 4(a), demonstrating the presence of rotational/transversal twins. (d) Profile intensity scan along the direction of the arrow shown in Figure 4(c), confirming that the dumbbells are As-terminated and hence the NW is B-polar. (e) Image of a section of a B-polar NW, showing the occurrence of twins and WZ segments. (f) The occurrence of a notch-like defect, initiating a polarity reversal to the A-polar direction on the right, as opposed to the normal B-polar growth on the left of the image. (g) Configuration of the NW shown in Figure 4(a) under the droplet. Note that the images in Figures 4 (a) to (d) , (e), and (f) to (g) are taken from different NWs.

This journal is © The Royal Society of Chemistry 20xx

Please do not adjust margins

Please do not adjust margins

Nanoscale

ARTICLE

To elaborate on the structural and morphological differences of A and B-polar NWs, we refer to Figure 5. As mentioned previously, our A-polar NWs have an exceptionally clean and defect-free structure. This point is illustrated in Figure 5(a), in which, except for the areas close to the base, the generic A-polar NW shows defect-free, single-crystalline ZB structure. A reconstruction of this NW obtained by stitching multiple HRTEM images is given in the Supporting information (SI), Figure SI1. No twinning is observed in the body of this NW.

The presence of a region of competing and mixed polarities has important implications on the morphology of A- polar NWs. Comparing Figures 3(a) and 4(a), one can see that A-polar NWs are tapered, as opposed to the B-polar NWs. This tapering is also apparent in Figure 5(a). The detailed description of the cross-sectional evolution of A-polar NWs is presented in the SI. In short, after the polarity is stabilized to A, the NW has a hexagonal cross section that is stretched along one of its diagonals and hence is deviated from regular hexagonal shape. This geometry entails that the droplet has an ellipsoidal shape instead of a spherical shape. As growth continues, the droplet tries to adopt the energetically preferred spherical shape.[37] This transition to a spherical geometry drives the cross section to the regular hexagonal shape. We believe that the observed tapering is caused by this transition.

For B-polar NWs, we observe that the body of the NW is composed of twined ZB phase with inclusions of WZ phase. Excluding the exceptional cases such as the one depicted in Figures 4(f) and 4(g), B-polar NWs obtained under these conditions are always terminated by the WZ segment, which is compatible with the previous observations.[45,46] The cooling down process after growth is carried out under the As flux in order to prevent the decomposition of GaAs at the high growth temperature.[47,48] This effectively imposes an increased V/III ratio during the growth termination, which favors WZ phase formation.[49,50]

For gold-catalyzed GaAs NWs, it has been previously reported that A-polar NWs have higher contact angles compared to their B-polar counterparts.[26] However, we did not observe any significant difference in the contact angles of A and B-polar NWs. We define here the contact angle β defined between the droplet surface at the corner of the nanowire and the overall growth surface (see sketch in Figure. 5). It does not consider the existence of a truncation. These values are obtained by ex-situ measurements. The detailed explanation about the reason for having similar contact angles in A and B-polar NWs is presented in the SI.

The exceptional crystal quality of A-polar NWs, with the effective absence of the WZ phase or twinning defects, calls for discussion. To understand the reason for the observed structural difference of A and B-polar NWs, we compare the geometries of their growth interfaces. The images shown in Figures 5(b) and (c) reveal the truncated growth front in A-polar NWs, with almost symmetrical inward tapered edge facets that are wetted by the droplet. Conversely, the growth front of B-polar NWs is always planar, and vertical sidewalls of such NWs are not wetted by the droplet. According to the current view,[50,51] the truncation develops when the surface energy change of forming the truncation, $\Delta\gamma$, is negative, while positive $\Delta\gamma$ yields the planar growth interface. This $\Delta\gamma$ has the form

$$\Delta\gamma = \frac{\gamma_{0L}}{\cos\theta} - \gamma_{SL}\tan\theta - \gamma_{0V} + \gamma_{LV}\sin\beta \,. \quad (1)$$

According to this expression, the surface energy change contains the solid-liquid energy of the created inward tapered facet $\gamma_{0L}/\cos\theta$ making the angle θ to the NW axis (see sketch in Figure. 5 for θ), the increased area of the liquid-vapor interface $\gamma_{LV}\sin\beta$ and the two surface energies of the straight solid-vapor facet parallel to the NW axis ($-\gamma_{0V}$) and the (111) solid-liquid top facet ($-\gamma_{SL}\tan\theta$) eliminated by truncation. As mentioned above, the contact angles of the gallium droplets on top of A and B-polar NWs are very similar, which is why the last term in the equation can be considered identical. The side facets of both types of NWs, as well as the inward tapered facets, should also have very close atomic arrangements. Therefore, the main difference may originate from the different energies of the (111)A and (111)B top facets in contact with liquid, where the energy of the (111)A facet is expected to be larger according to the earlier discussion. This explains why, even for the same contact angles, the $-\gamma_{SL}\tan\theta$ term favors the truncation in A-polar NWs and suppresses it in B-polar NWs.

Whenever the truncation is present, it cannot grow infinitely according to Ref. 50, but rather adopts the energetically preferred size which oscillates in synchronization with the monolayer growth cycle. The droplet sliding down along the straight sidewalls is energetically suppressed.[36] Therefore, the droplet is stable on top of the truncated A-polar NW. If all NW facets are truncated, as suggested by the image in Figure 5 (b), nucleation of two-dimensional islands does not occur at the triple phase line (TPL), but rather in the center of the liquid-solid interface.[36,51] No WZ or twin formation is expected in this nucleation regime, because the islands are stable against either 60° or 30° rotation (producing the WZ phase or twins, respectively). In contrast to A-polar NWs, the island nucleation in B-polar NWs occurs at the TPL. In this case, the WZ islands or twinning defects emerge with a certain probability which depends on the chemical potential.[23,26] High chemical potentials

Please do not adjust margins

Please do not adjust margins

would favor predominantly WZ phase.[36] However, due to the low V/III ratios employed in our growths, the chemical potential values are quite low, which explains the random occurrence of the WZ phase or twins in our B-polar NWs. This picture is fully consistent with all of our experimental observations and correlates with the results of Ref. 49, where the truncated growth front in Ga-assisted GaAs NWs was also observed at low V/III ratios. The increase in the population of A-polar NWs for low V/III ratios can be explained by the fact that the truncated growth fronts that are required for the growth of these wires are more favored to be formed in these V/III ratios.

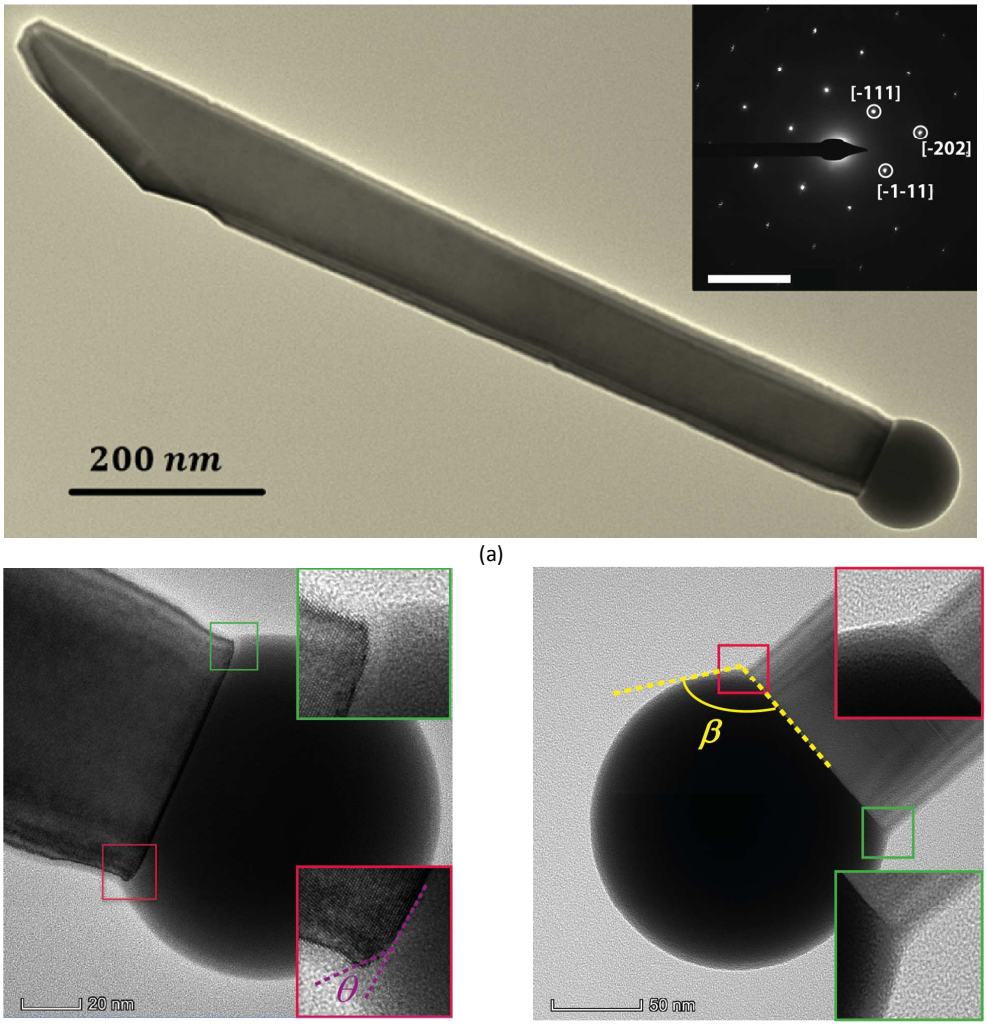

Figure 5. (a) Low magnification bright field TEM image of an A-polar NW. The inset shows the diffraction pattern corresponding to the ZB phase, with the scale bar in the inset being 5 1/nm. (b) The droplet configuration of the A-polar NW shown in (a). The red and green insets depict the truncated growth front. (c) The droplet configuration of a B-polar NW, in which the growth front is always planar. These images are taken in [101] zone axis. The NWs depicted in Figures 5(a),(b) and (c) are grown at a V/III ratio of 4.6 and a 2D-equivalent growth rate of 0.27 Å/s; the SEM image of as-grown sample is presented in Fig. SI4(a). Note that the slight roughening of the NW sidewalls in (a) is caused by gradual oxidation of the GaAs, and is not a product of the growth process itself.

This journal is © The Royal Society of Chemistry 20xx

Please do not adjust margins

Please do not adjust margins

Nanoscale

ARTICLE

Finally, we demonstrate the functionality of A-polar NWs by characterizing their optical properties. We measured the light emission of the NWs by CL at 20 K directly on an as-grown sample, and also on NWs dispersed on TEM grids. As stated above, the NWs were capped by the $AlAs/Al_{0.33}Ga_{0.66}As$ / $GaAs$ structure, yielding the formation of optically active (Al)GaAs QDs. We now correlate their occurrence and brightness with the polarity of the host NW.[40]

Figure 6 presents the typical CL measurements. Figure 6(a) shows the SEM micrograph of the investigated region, with the two polarities indicated by the corresponding arrows. Figure 6(b) shows the panchromatic image of the CL signal, indicating that NWs with A-polarity have much more uniform emission intensity. Figure 6(c) shows the emission mapping, color-coded into the three main emission wavelengths: 822, 836 and 854 nm, corresponding 1.51, 1.48 and 1.45 eV, respectively. The lowest wavelength corresponds to the free exciton emission of GaAs at 20 K, while the longer wavelengths can be attributed to the carbon contamination and polytypism.[24] Between 820 and 860 nm, A-polar NWs show homogeneous emission.

We now analyze the emission spectra of the NWs. Figures 6 (e-h) show representative emission spectra in the 1.41-1.53 eV and 1.77-1.9 eV ranges. They were acquired from the two NWs with A and B polarities, with diameters of around 260 nm. For each NW, spectra 1 to 3 correspond to excitation along the NW at three different points from the base to the top. We first focus on the first emission range, corresponding to the GaAs core emission. Considering an A-polar NW, the spectrum is clearly formed by two peaks, centered at 1.51 eV and 1.48 eV. For this particular NW, the low-energy peak increases in intensity toward the NW top. The spectra of B-polar NWs are much broader and red-shifted with respect to the free exciton emission of GaAs.

To understand this drastically different optical behavior of the cores of A and B-polar NWs, we note that planar defects, such as stacking faults and twins, effectively introduce unitary WZ sections in the ZB phase (and vice versa). The ZB/WZ GaAs heterostructure are known to have staggered type-II band alignment,[52–55] which localizes electrons in the ZB and holes in the WZ segments. As a result, the core emission redshifts, which has been previously shown to depend on the density of defects.[46] There is almost no intensity at 1.51 eV for B-polar NWs, as expected for polytypic structures.[24] Furthermore, while the stacking faults and twins can act as effective traps for the carriers moving axially in the NWs, they allow for charge transfer perpendicular to the NW axis.[56] The radial transport of the trapped carriers can broaden the excitonic emission by a fluctuating Stark effect.[56,57] In addition, by limiting the charge transport to the radial direction, these defects deplete the shell from excitons by favoring their transfer into the core, according to the gradient of the band gap between the core and the shell.[58] In summary, the effects of structural defects on the core emission of B-polar NWs with respect to defect-free A-polar NWs manifest in (i) spectral broadening of the emission, (ii) an increased emission intensity of the core, and (iii) redshift of the emission. The narrower blue-shifted emission lines from A-polar NWs are compatible with their higher crystal quality.

We now address the existence of a clear low-energy peak in the spectra of A-polar GaAs NWs at 1.48 eV. In order to ensure a better spatial resolution for observing the two peaks, we investigated the NWs on a TEM grid. Figure 6(i) maps the emission at 1.51 eV, 1.48 eV, and 1.44 eV. The intensities are normalized for clear determination of the different regions. We observe that the free exciton emission at 1.51 eV is detected mainly when exciting the NWs core. The excitation map in the external regions of the NW shows two emission peaks at 1.48 eV and 1.51 eV. We note the peak at 1.48 is more prominent. The emission at 1.48 eV has previously been attributed to carbon.[59–62] We believe that the carbon incorporation at the NW surface can occur during the CL investigation. We also note that a weak emission at 1.48 eV is also observable upon excitation of the NW core, which should be due to diffusion and recombination of some excitons in the shell.

Emission at longer wavelengths can be observed only in the NW top. This can be attributed to fluctuations in the growth chamber at the very end of the growth, leading to morphological instabilities.

This journal is © The Royal Society of Chemistry 20xx

Please do not adjust margins

Please do not adjust margins

Nanoscale

ARTICLE

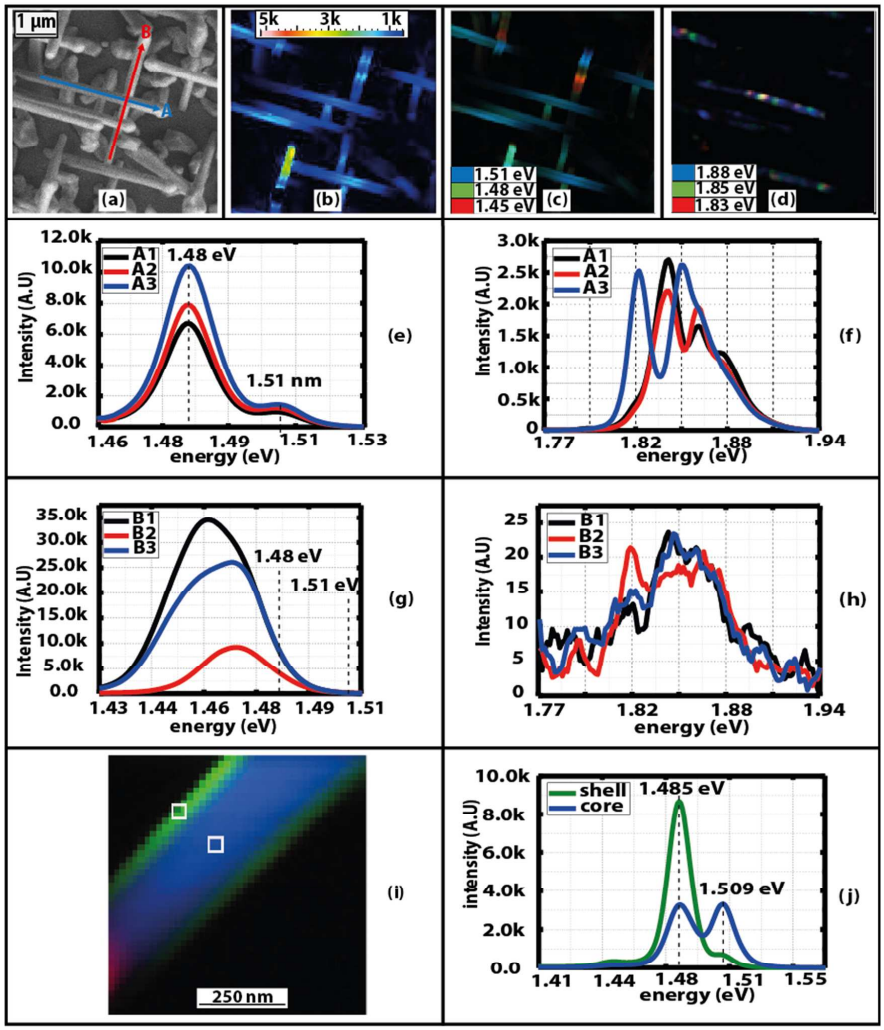

Figure 6. Characterization of the optical properties of NWs with A and B-polarities using CL at 20 K. (a) Top view SEM image captured inside the CL microscope. The arrows indicate the directions of the two different polarities. (b) Panchromatic intensity map for the identical image frame. (c) and (d) The wavelength-dependent CL intensity map of the same region. (e) and (f) CL emission spectra collected from the three points of an A-polar NW, in the ranges 1.46-1.53 eV and 1.77-1.94 eV. The two ranges correspond to the emission from the GaAs core and the AlGaAs shell, respectively. (g) and (h) CL emission spectra collected from the three points of a B-polar NW (i) High-magnification wavelength-dependent map obtained on an A-polar NW lying on a TEM grid. The color code is the same as in (c). (j): CL spectra collected from the points indicated in the NW core and shell.

Please do not adjust margins

Please do not adjust margins

Finally, we study the second emission range (1.77-1.94 eV), which corresponds to the emission from the AlGaAs shell, as a function of the core polarity. It has previously been shown that compositional fluctuations in AlGaAs result in the formation of QDs that emit in the range between 1.77 eV and 1.94 eV nm.[40,63] In CL, these QDs appear as spatially localized emitters.[40,63] Figure 6(d) compares the CL mapping of A and B-polar NWs in the QD spectral region. Under these excitation conditions, we can find many spots of localized emission for most of A-polar NWs, while there is no significant emission from B-polar NWs. Representative emission spectra of A and B-polar NWs are compared in Figures 6 (f) and (h). The QD-like emission around 1.85 eV is observed in both cases, with the emission of A-polar NWs being much brighter. As discussed earlier, defects in B-polar NWs act as the shortcuts for injecting excitons from the shell to the core. This migration depletes the QDs from excitons in B-polar NWs. The much lower density of defects in A-polar NWs means that the excitons remain in the QDs, which is why the QD emission in these NWs shows two orders of magnitude higher the intensity with respect to B-polar NWs. This enhancement is observable in Figures 6(d), 6(f) and 6(h).

Conclusions

In conclusion, we have reported an optimized growth of A-polar GaAs NW on GaAs(100) substrates by the Ga-assisted VLS method. Decreasing the V/III flux ratio has been found crucial for improving the yield of A-polar NWs up to 57%. Similar to the Au-catalyzed VLS method, A-polar GaAs NWs are generally free of stacking defects along their entire length, while B-polar NWs suffer from random twining and WZ insertions. Exceptional crystal quality of A-polar NWs is understood through the truncated geometry of their growth interface, which suppresses the TPL nucleation and hence the formation of stacking faults. We speculate that the truncation develops in A-polar NWs due to the higher surface energy of the top (111)A facet with respect to the (111)B one. We have correlated the optical properties of the NWs with their polarity. Luminescence from A-polar NWs is homogeneous along the NW, with an intense peak around 1.51 eV (820 nm). This peak corresponds to the free exciton in ZB GaAs, in agreement with the higher crystal quality of A-polar NWs. The effect of crystal quality of the host NW on the emission properties of AlGaAs QDs in the shell has been shown for the first time. The QD emission from the AlGaAs shells is two orders of magnitude brighter in A-polar NWs. This is explained by a larger number of excitons in QDs surrounding such NWs. This opens a clear path toward the fabrication of bright QDs in GaAs, which have many promising applications in optoelectronic devices.

This work opens many novel fundamental questions in the current understanding and state-of-the-art of nanowire growth as well as new avenues for crystal-phase and growth direction engineering.

Conflicts of interest

There are no conflicts to declare.

Acknowledgements

The funding for this research was provided by Swiss National Science Foundation (SNSF), National Centre of Competence in Research Quantum Science and Technology (NCCR QSIT) and Horizon 2020 European Union Funding for Research and Innovation through projects INDEED and LIMQUET. The authors express their gratitude to the staff of EPFL's Interdisciplinary Center for Electron Microscopy (CIME), particularly Dr Davide Deiana, for the support. SMS acknowledges funding from "Programa Internacional de Becas "la Caixa"-Severo Ochoa". SMS and JA acknowledge funding from Generalitat de Catalunya 2017 SGR 327 and the Spanish MINECO ENE2017-85087-C3-3-R project. ICN2 acknowledges support from the Severo Ochoa Program (MINECO, Grant SEV-2013-0295) and is funded by the CERCA Programme / Generalitat de Catalunya. Part of the present work has been performed in the framework of Universitat Autònoma de Barcelona Materials Science PhD program. Part of the HAADF-STEM microscopy was conducted in the Laboratorio de Microscopias Avanzadas at the Instituto de Nanociencia de Aragon-Universidad de Zaragoza. JA and SMS thank them for offering access to their instruments and expertise. This work has received funding from the European Union's Horizon 2020 Research and Innovation Programme under grant agreement No. 654360 NFFA-Europe. VGD thanks the Russian Foundation for Basic Research for financial support under grants 17-52-16017, 16-29-03129, 16-02-00134, 16-29-03283, and 18-02-40006.

Notes and references

1 R. S. Wagner and W. C. Ellis, *Appl. Phys. Lett.*, 1964, **4**, 89–90.

2 M. Takahasi, M. Kozu and T. Sasaki, *Jpn. J. Appl. Phys.*, 2016, **55**, 04EJ04.

3 Z. H. Wu, X. Y. Mei, D. Kim, M. Blumin and H. E. Ruda, *Appl. Phys. Lett.*, 2002, **81**, 5177–5179.

4 P. Schroth, J. Jakob, L. Feigl, S. M. Mostafavi Kashani, J. Vogel, J. Strempfer, T. F. Keller, U. Pietsch and T. Baumbach, *Nano Lett.*, 2018, **18**, 101–108.

5 M. Takahasi, M. Kozu, T. Sasaki and W. Hu, *Cryst. Growth Des.*, 2015, **15**, 4979–4985.

6 D. V. Lang, H. G. Grimmeiss, E. Meijer and M. Jaros, *Phys. Rev. B*, 1980, **22**, 3917–3934.

7 J. Tersoff, *Nano Lett.*, 2015, **15**, 6609–6613.

8 P. Krogstrup, R. Popovitz-Biro, E. Johnson, M. H. Madsen, J. Nygård and H. Shtrikman, *Nano Lett.*, 2010, **10**, 4475–4482.

9 B. Mandl, J. Stangl, E. Hilner, A. A. Zakharov, K. Hillerich, A. W. Dey, L. Samuelson, G. Bauer, K. Deppert and A. Mikkelsen, *Nano Lett.*, 2010, **10**,

Formatted: German (Germany)

Formatted: German (Germany)

Please do not adjust margins

Please do not adjust margins

4443–4449.

10 S. J. Gibson, J. P. Boulanger and R. R. LaPierre, *Semicond. Sci. Technol.*, 2013, **28**, 105025.

11 B. Bauer, A. Rudolph, M. Soda, A. Fontcuberta i Morral, J. Zweck, D. Schuh and E. Reiger, *Nanotechnology*, 2010, **21**, 435601.

12 S. Ambrosini, M. Fanetti, V. Grillo, A. Franciosi and S. Rubini, *J. Appl. Phys.*, 2011, **109**, 094306.

13 C. Colombo, D. Spirkoska, M. Frimmer, G. Abstreiter and A. Fontcuberta i Morral, *Phys. Rev. B*, 2008, **77**, 155326.

14 A. Fontcuberta i Morral, C. Colombo, G. Abstreiter, J. Arbiol and J. R. Morante, *Appl. Phys. Lett.*, 2008, **92**, 063112.

15 M. de la Mata, C. Magen, J. Gazquez, M. I. B. Utama, M. Heiss, S. Lopatin, F. Furtmayr, C. J. Fernández-Rojas, B. Peng, J. R. Morante, R. Rurali, M. Eickhoff, A. Fontcuberta i Morral, Q. Xiong and J. Arbiol, *Nano Lett.*, 2012, **12**, 2579–2586.

16 F. Schuster, M. Hetzl, S. Weiszer, J. A. Garrido, M. de la Mata, C. Magen, J. Arbiol and M. Stutzmann, *Nano Lett.*, 2015, **15**, 1773–1779.

17 M. I. B. Utama, F. J. Belarre, C. Magen, B. Peng, J. Arbiol and Q. Xiong, *Nano Lett.*, 2012, **12**, 2146–2152.

18 M. de la Mata, R. Leturcq, S. R. Plissard, C. Rolland, C. Magén, J. Arbiol and P. Caroff, *Nano Lett.*, 2016, **16**, 825–833.

19 M. de la Mata, C. Magén, P. Caroff and J. Arbiol, *Nano Lett.*, 2014, **14**, 6614–6620.

20 F. Schuster, B. Laumer, R. R. Zamani, C. Magén, J. R. Morante, J. Arbiol and M. Stutzmann, *ACS Nano*, 2014, **8**, 4376–4384.

21 M. I. B. Utama, M. de la Mata, C. Magen, J. Arbiol and Q. Xiong, *Adv. Funct. Mater.*, 2013, **23**, 1636–1646.

22 H. Potts, Y. van Hees, G. Tütüncüoglu, M. Friedl, J.-B. Leran and A. Fontcuberta i Morral, *Cryst. Growth Des.*, 2017, **17**, 3596–3605.

23 F. Glas, J.-C. Harmand and G. Patriarche, *Phys. Rev. Lett.*, 2007, **99**, 146101.

24 D. Spirkoska, J. Arbiol, A. Gustafsson, S. Conesa-Boj, F. Glas, I. Zardo, M. Heigoldt, M. H. Gass, A. L. Bleloch, S. Estrade, M. Kaniber, J. Rossler, F. Peiro, J. R. Morante, G. Abstreiter, L. Samuelson and A. Fontcuberta i Morral, *Phys. Rev. B*, 2009, **80**, 245325.

25 I. Zardo, S. Conesa-Boj, F. Peiro, J. R. Morante, J. Arbiol, E. Uccelli, G. Abstreiter and A. Fontcuberta i Morral, *Phys. Rev. B*, 2009, **80**, 245324.

26 X. Yuan, P. Caroff, J. Wong-Leung, L. Fu, H. H. Tan and C. Jagadish, *Adv. Mater.*, 2015, **27**, 6096–6103.

27 I. Forrest M. Davidson, Doh C. Lee, A. Dayne D. Fanfair and B. A. Korgel, *J.Phys.Chem. C*, 2007, **111**, 2929–2935.

28 R. R. Zamani, S. Gorji Ghalamestani, J. Niu, N. Sköld and K. A. Dick, *Nanoscale*, 2017, **9**, 3159–3168.

29 A. Fontcuberta i Morral, J. Arbiol, J. D. Prades, A. Cirera and J. R. Morante, *Adv. Mater.*, 2007, **19**, 1347–1351.

30 K. W. Schwarz and J. Tersoff, *Nano Lett.*, 2011, **11**, 316–320.

31 Y. Yuan and T. R. Lee, in *Surface Sciecne Techniques*, 2013, pp. 3–34.

32 F. Matteini, G. Tütüncüoglu, D. Mikulik, J. Vukajlovic-Plestina, H. Potts, J.-B. Leran, W. C. Carter and A. Fontcuberta i Morral, *J. Cryst. Growth*, 2016, **16**, 5781–5786.

33 F. Matteini, G. Tütüncüoğlu, D. Rüffer, E. Alarcón-Lladó and A. Fontcuberta i Morral, *J. Cryst. Growth*, 2014, **404**, 246–255.

34 F. Matteini, G. Tütüncüoglu, D. Mikulik, J. Vukajlovic-Plestina, H. Potts, J.-B. Leran, W. C. Carter and A. Fontcuberta i Morral, *Cryst. Growth Des.*, 2016, **16**, 5781–5786.

35 F. Matteini, G. Tütüncüoglu, H. Potts, F. Jabeen and A. Fontcuberta i Morral, *Cryst. Growth Des.*, 2015, **15**, 3105–3109.

36 V. G. Dubrovskii, *Cryst. Growth Des.*, 2017, **17**, 2589–2593.

37 J. Berthier and K. A. Brakke, *The physics of microdroplets*, John Wiley & Sons, Inc, 2012.

38 N. Moll, A. Kley, E. Pehlke and M. Scheffler, *Phys. Rev. B*, 1996, **54**, 8844–8855.

39 J. Wang, S. R. Plissard, M. A. Verheijen, L.-F. Feiner, A. Cavalli and E. P. A. M. Bakkers, *Nano Lett.*, 2013, **13**, 3802–3806.

40 M. Heiss, Y. Fontana, A. Gustafsson, G. Wüst, C. Magen, D. D. O'Regan, J. W. Luo, B. Ketterer, S. Conesa-Boj, A. V. Kuhlmann, J. Houel, E. Russo-Averchi, J. R. Morante, M. Cantoni, N. Marzari, J. Arbiol, A. Zunger, R. J. Warburton and A. Fontcuberta i Morral, *Nat. Mater.*, 2013, **12**, 439–444.

41 Ramsdell L.S, *Am. Mineral.*, 1945, **32**, 64–82.

42 A. M. Sanchez, Y. Zhang, E. W. Tait, N. D. M. Hine, H. Liu and R. Beanland, *Nano Lett.*, 2017, **17**, 2454–2459.

43 S. Conesa-Boj, I. Zardo, S. Estradé, L. Wei, P. Jean Alet, P. Roca i Cabarrocas, J. R. Morante, F. Peiró, A. F. i Morral and J. Arbiol, *Cryst. Growth Des.*, 2010, **10**, 1534–1543.

44 J. Arbiol, A. Fontcuberta i Morral, S. Estradé, F. Peiró, B. Kalache, P. Roca i Cabarrocas and J. R. Morante, *J. Appl. Phys.*, 2008, **104**, 064312.

45 F. Jabeen, V. Grillo, S. Rubini and F. Martelli, *Nanotechnology*, 2008, **19**, 275711.

46 M. Heiss, S. Conesa-Boj, J. Ren, H.-H. Tseng, A. Gali, A. Rudolph, E. Uccelli, F. Peiró, J. R. Morante, D. Schuh, E. Reiger, E. Kaxiras, J. Arbiol and A. Fontcuberta i Morral, *Phys. Rev. B*, 2011, **83**, 045303.

47 T. E. Haynes, W. K. Chu, T. L. Aselage and S. T. Picraux, *Appl. Phys. Lett.*, 1986, **49**, 666–668.

48 J. Tersoff, D. E. Jesson and W. X. Tang, *Phys. Rev. Lett.*, 2010, **105**, 035702.

49 W. Kim, V. G. Dubrovskii, J. Vukajlovic-Plestina, G. Tütüncüoglu, L. Francaviglia, L. Güniat, H. Potts, M. Friedl, J.-B. Leran and A. Fontcuberta i Morral, *Nano Lett.*, 2018, **18**, 49–57.

50 D. Jacobsson, F. Panciera, J. Tersoff, M. C. Reuter, S. Lehmann, S. Hofmann, K. A. Dick and F. M. Ross, *Nature*, 2016, **531**, 317–322.

51 C.-Y. Wen, J. Tersoff, K. Hillerich, M. C. Reuter, J. H. Park, S. Kodambaka, E. A. Stach and F. M. Ross, *Phys. Rev. Lett.*, 2011, **107**, 025503.

52 P. Krogstrup, M. Hannibal Madsen, W. Hu, M. Kozu, Y. Nakata, J. Nygård, M. Takahasi and R. Feidenhans'l, *Appl. Phys. Lett.*, 2012, **100**, 093103.

53 P. Kusch, E. Grelich, C. Somaschini, E. Luna, M. Ramsteiner, L. Geelhaar, H. Riechert and S. Reich, *Phys. Rev. B*, 2014, **89**, 045310.

54 L. Ahtapodov, H. Kauko, A. M. Munshi, B. O. Fimland, A. T. J. van Helvoort and H. Weman, *J. Appl. Phys.*, 2017, **122**, 245102.

Formatted: French (France)

Formatted: German (Germany)

Formatted: German (Germany)

This journal is © The Royal Society of Chemistry 20xx

Please do not adjust margins

Please do not adjust margins

55 D. Spirkoska, A. L. Efros, W. R. L. Lambrecht, T. Cheiwchanchamnangij, A. Fontcuberta i Morral and G. Abstreiter, *Phys. Rev. B*, 2012, **85**, 045309.

56 D. Dalacu, K. Mnaymneh, J. Lapointe, X. Wu, P. J. Poole, G. Bulgarini, V. Zwiller and M. E. Reimer, *Nano Lett.*, 2012, **12**, 5919–5923.

57 G. Sallen, A. Tribu, T. Aichele, R. André, L. Besombes, C. Bougerol, S. Tatarenko, K. Kheng and J. P. Poizat, *Phys. Rev. B*, 2009, **80**, 085310.

58 J. Nelson, The Physics Of Solar Cells.

59 G. Tütüncüoglu, EPFL, 2017.

60 Hannah Jane Joyce, Australian National University, 2009.

61 B. J. Skromme and G. E. Stillman, *Phys. Rev. B*, 1984, **29**, 1982–1992.

62 B. J. Skromme, T. S. Low, T. J. Roth, G. E. Stillman, J. K. Kennedy and J. K. Abrokwah, *J. Electron. Mater.*, 1983, **12**, 433–457.

63 L. Francaviglia, Y. Fontana, S. Conesa-Boj, G. Tütüncüoglu, L. Duchêne, M. B. Tanasescu, F. Matteini and A. Fontcuberta i Morral, *Appl. Phys. Lett.*, 2015, **107**, 033106.

This journal is © The Royal Society of Chemistry 20xx

Please do not adjust margins

Supporting information: Optimizing the yield of A-polar GaAs nanowires to achieve defect-free zinc blende structure and enhanced optical functionality

M. Zamani et al

HRTEM Reconstruction of A-polar NWs

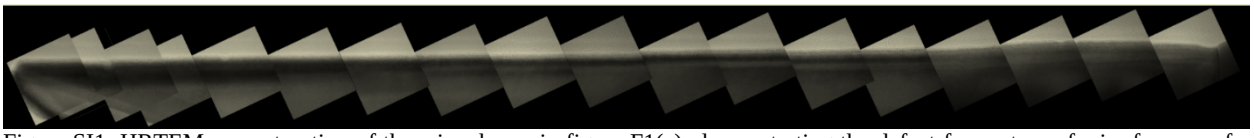

Figure SI1: HRTEM reconstruction of the wire shown in figure F1(a), demonstrating the defect-free nature of wire for areas far from the root.

Discussion on the Morphology of A-polar NWs

To understand the tapering of the A-polar wires, low magnification HAADF-STEM images are used. In this imaging mode, the intensity is proportional to $z^{\alpha}h$, in which z and h are the atomic number and the thickness of the specimen [1] and $1 < \alpha < 2$. When probing GaAs NWs, one can use the variation of the HAADF intensity to probe the thickness variation of the cross section of the NWs. Figure SI2(a) shows one such HAADF image. Figure SI2(b) shows an schematic view of the hexagonal cross section of the nanowire, while figure SI2(c) demonstrates the scan profile corresponding to point P9.

In order to characterize the cross section, we define these geometrical parameters:

$$l = AD, l' = BC = EF,\ h = BF = CE$$

The aspect ratio is defined as:

$$a = \frac{l - l'}{l'} = \frac{l}{l'} - 1$$

For a perfectly regular hexagon, this aspect ratio will be equal to one. We notice that for $l = l'$, the aspect ratio will be zero and the cross section will have a rectangular shape. Aspect ratios less than one show elongation along AD direction, as shown in Figure SI2(b).

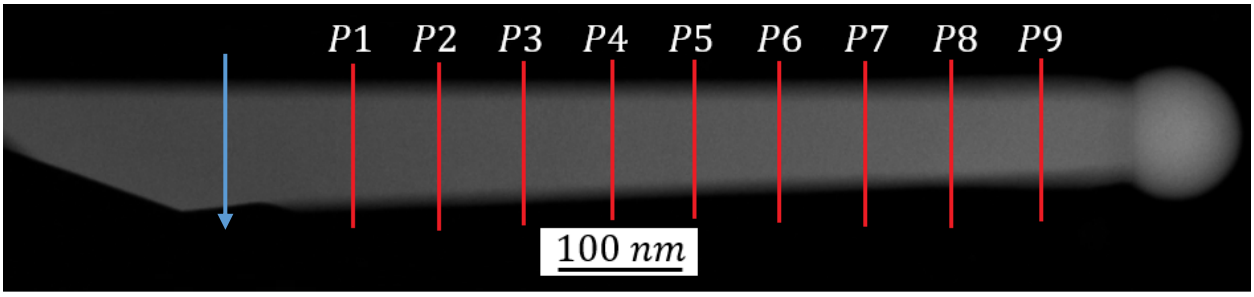

Supporting information: Optimizing the yield of A-polar GaAs nanowires to achieve defect-free zinc blende structure and enhanced optical functionality

M. Zamani et al

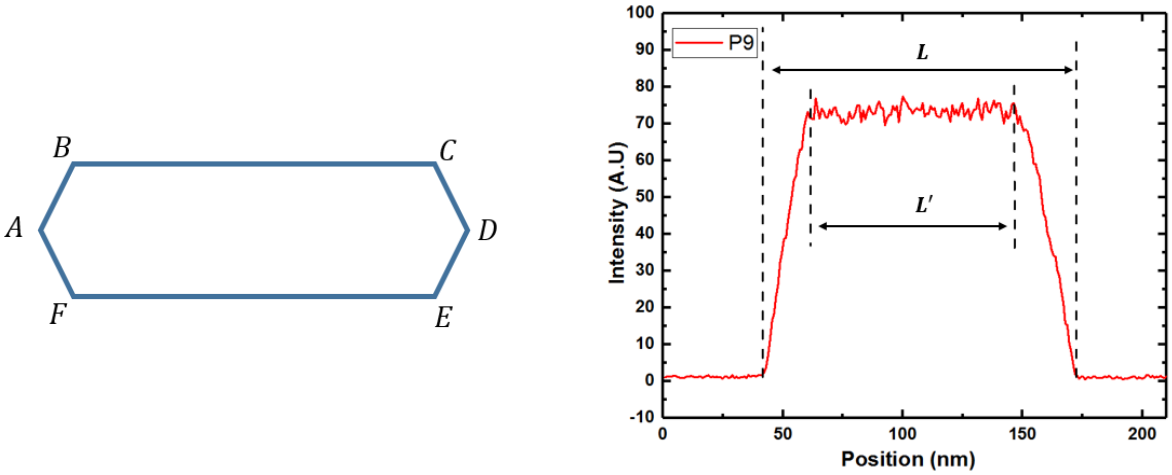

Figure SI2. (a) low magnification HAADF image of an A-polar wire used to extract the geometrical parameters of the cross section. (b) schematic view of the cross section of an A-polar wire.(c) profile scan corresponding to P9, demonstrating the determination of the parameters l and l'.The scan is done in the direction of the blue arrow in Figure S1(a).

Figure SI3 summarizes the variation of the geometrical parameters of the cross section for points P1 to P9 as shown. This graph indicates that areas close to the root of the root of the NW, the aspect ratio is less than one and the hexagonal cross section is stretched along the along its AD diagonal. This cross section entails that the Ga droplet that drives the growth is ellipsoidal rather than spherical. It is well known that the droplets in contact with solid prefer to adopt spherical shapes, as spherical shape minimizes the total surface for a given volume, hence minimizing the total surface energy. As the nanowire growth continues, the droplet gradually tries to morph into spherical shape, and this causes the cross section of the nanowire to approach a regular hexagon shape. This process happens by reduction in both l and l', which is in turn responsible for the tapered shape of the nanowire. We notice that for point P9, the aspect ratio is very close to one and the cross section is close to a regular hexagon. The thickness of the hexagonal cross section for this point is then calculated assuming a perfectly regular hexagon with geometrical parameters l and l'. The cross section thickness for other points is then calculated using the relative intensity of HAADF scans for those points compared to point P9. We observe that the reduction in l and l' is accompanied by an increase in the thickness. This indicates the NWs have low thicknesses in the areas close to the root.

Supporting information: Optimizing the yield of A-polar GaAs nanowires to achieve defect-free zinc blende structure and enhanced optical functionality

M. Zamani et al

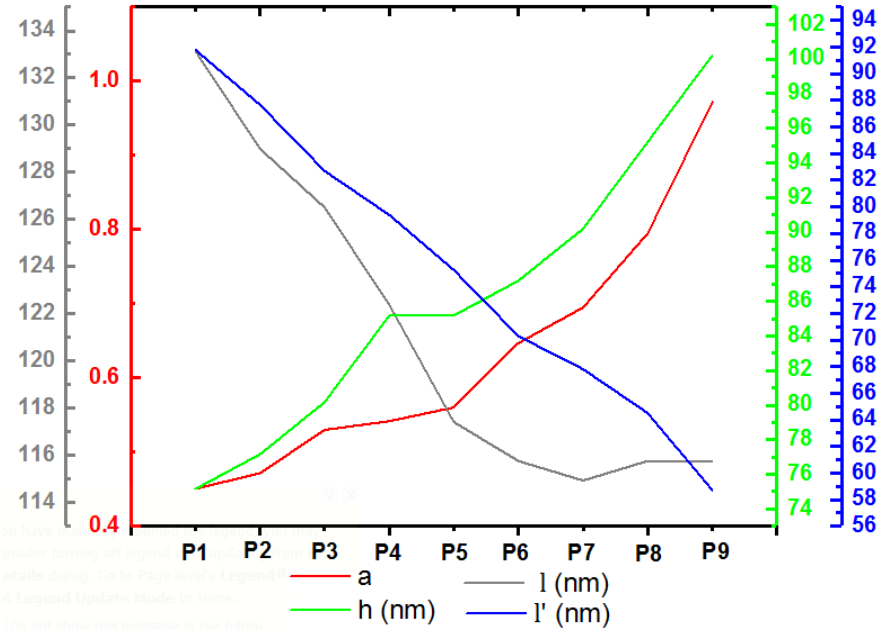

Figure SI3. Decrease in values of l and l' and increase in thickness and aspect ratio of the nanowire growth progresses from point P1 to P9. Reduction in l is responsible for the tapered shape of the NW, while the increase in the aspect ratio and the thickness of the wire indicate that the cross section approaches a regular hexagon shape as growth is progressed.

SEM images of samples discussed in the manuscript:

Supporting information: Optimizing the yield of A-polar GaAs nanowires to achieve defect-free zinc blende structure and enhanced optical functionality

M. Zamani et al

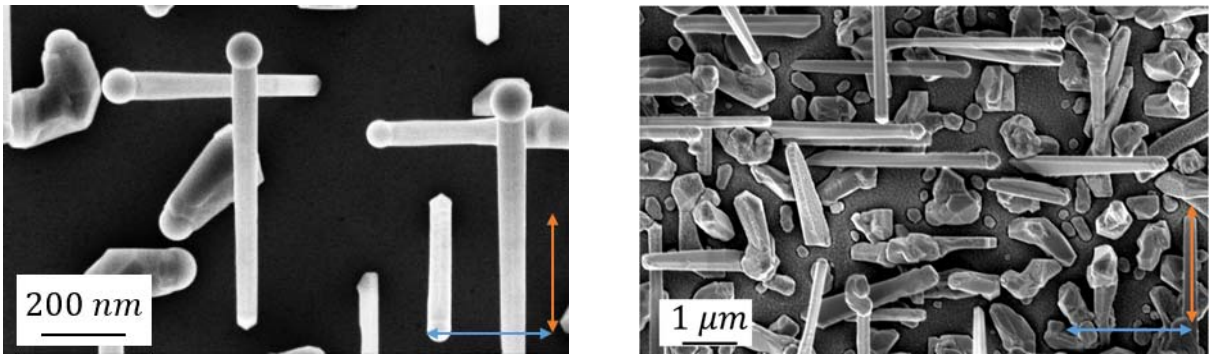

(a) (b)

Figure SI4. (a) and (b):Top view SEM image of sample discussed in Figure 5 and the core-shell sample discussed in Figure 6, respectively. The blue arrow shows the [111]A direction, while the orange arrow depict the [111]B.

Supporting information: Optimizing the yield of A-polar GaAs nanowires to achieve defect-free zinc blende structure and enhanced optical functionality

M. Zamani et al

Discussion on the insufficiency of ex-situ contact angle measurements

To reconcile the contradiction between our observations and the previously reported data, we refer to Figure 5(a) and 5(b) that depict the droplet configuration for A and B-polar NWs. We observe that the A-polar NWs are marked by a sudden shrinking in their diameter just below the droplet. This consistent characteristic of A-polar wires is absent in B-polar NWs. Figure SI4(a) and SI4(b) schematically demonstrate this behaviour. In this figure, the contact angles of A and B-polar NWs are depicted by α_A and α_B, respectively, while β_A shows the angle that the truncated growth front makes with the droplet. We note that, $\beta_A \cong \beta_A$ and $\alpha_A < \beta_B$. This implies that that, the truncated facet has higher surface energy than the B-polar surface.

The reduction in the diameters inadvertently imposes a sudden shrinking of the Ga droplet in A-polar NWs and this means that the contact angles measured by the ex-situ measurements might not be the same as the contact angles during the growth. As already mentioned, it has been previously discussed in the literature that central nucleation and formation of ZB phase happen at higher contact angles compared to TLP nucleation and WZ formation. However, the fact the last grown monolayers in A and B-polar wires show different nucleation mechanism and phases while having similar contact angle implies that the contact angle might not be sufficient to discriminate different growth mechanism in all the cases. Central nucleation and presence of truncated facets are believed to be necessary for formation of ZB [2,3]. As previously discussed, ZB phase is more favoured in low V/III ratios. This entails that increasing the V/III ratio at the last stage of growth makes the truncated growth front to become unfavourable. The shrinking of the diameter in A-polar NWs is caused by the fact that, at end stages of growth, the V/III ratio increases and the truncated facets start to disappear. This makes us believe that the truncated facets are bigger during the growth compared to what is observable in ex-situ setting. Since the B-polar wires are terminated by WZ phase, their growth front does not have any truncated facet and increased V/III does not change the geometry of their growth front. The absence of the shrinking behaviour in B-polar is a consequence of this fact. All in all, based on the discussions presented here, we conclude that a reasonable comparison of the contact angles in self-catalyzed GaAs NW growth is possible only by in-situ techniques. Even if not cooled down under As flux, different desorption rates of Ga and As atoms from the walls of the growth chamber and the sample will impose a change in the effective V/III ratio and cause a possible shift in the contact angle.

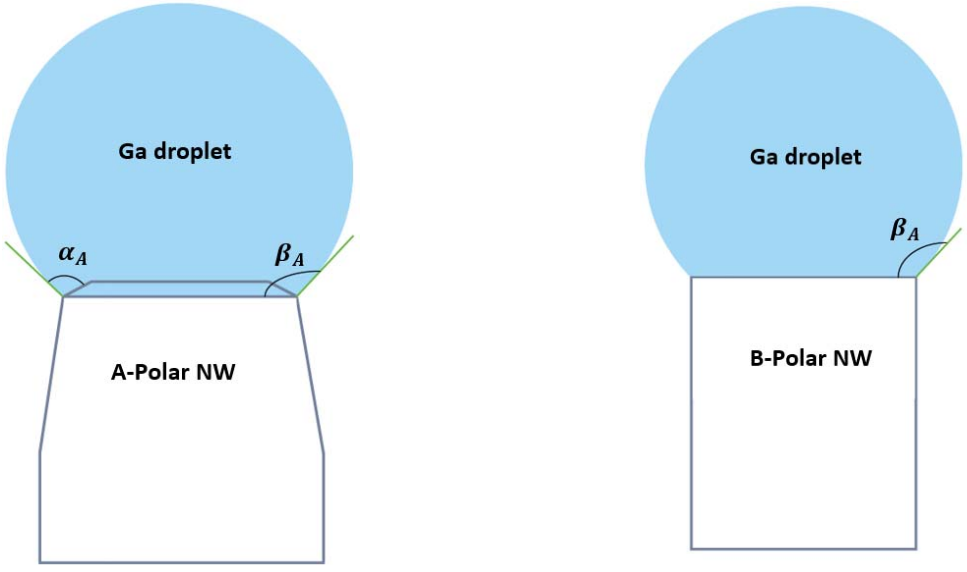

Figure SI(5): schematic view of the droplet configuration as observed by ex-situ setup for A and B-polar NWs.

1 C. B. Carter and D. B. Williams, Eds., *Transmission Electron Microscopy*, Springer International Publishing, Cham, 2016.

Supporting information: Optimizing the yield of A-polar GaAs nanowires to achieve defect-free zinc blende structure and enhanced optical functionality

M. Zamani et al

2 D. Jacobsson, F. Panciera, J. Tersoff, M. C. Reuter, S. Lehmann, S. Hofmann, K. A. Dick and F. M. Ross, *Nature*, 2016, **531**, 317–322.

3 C.-Y. Wen, J. Tersoff, K. Hillerich, M. C. Reuter, J. H. Park, S. Kodambaka, E. A. Stach and F. M. Ross, *Phys. Rev. Lett.*, 2011, **107**, 025503.

Contribution of authors:

Mahdi Zamani, Gözde Tütüncüoglu performed growth studies, transmission electron microscopy and cathodoluminescence

Sara Martí-Sánchez and Jordi Arbiol performed Cs corrected transmission electron microscopy measurements and analysis (supervision by J. Arbiol)

Luca Francaviglia and Edoardo Markov helped in cathodoluminescence studies

Lucas Güniat , Heidi Potts, Martin Friedl, Wonjong Kim, Jean-Baptiste Leran gave support in the growth studies

Lea Ghisalberti and Vladimir G. Dubrovskii provided theoretical analysis

Anna Fontcuberta i Morral supervised and coordinated the project

All authors have participated in the scientific discussion and writing of the manuscript